Conference or Workshop Item:
Wright, Marvin, Gorma, Wael, Luo, Yang et al. (3 more authors) (Accepted: 2020) Multi-actuated AUV Body for Windfarm Inspection: Lessons from the Bio-inspired RoboFish Field Trials. In: UNSPECIFIED. (In Press)

Multi-actuated AUV Body for Windfarm Inspection: Lessons from the Bio-inspired RoboFish Field Trials

Marvin Wright
Dept. of Naval Architecture Ocean & Marine Engineering Engineering
University of Strathclyde
Glasgow, United Kingdom
marvin.wright@strath.ac.uk

Wael Gorma
Dept. of Electronic Engineering
University of York
York, United Kingdom
wael.gorma@york.ac.uk

Yang Luo
Dept. of Naval Architecture Ocean & Marine Engineering Engineering
University of Strathclyde
Glasgow, United Kingdom
y.luo@strath.ac.uk

Mark Post
Dept. of Electronic Engineering
University of York
York, United Kingdom
mark.post@york.ac.uk

Qing Xiao
Dept. of Naval Architecture Ocean & Marine Engineering Engineering
University of Strathclyde
Glasgow, United Kingdom
qing.xiao@strath.ac.uk

Andrew Durrant
Dept. of R&D
PicSea Ltd.
Edinburgh, UK
andrew@picsea.co.uk

Abstract—An innovative magnetic joint design has been developed as part of the construction of a bio-inspired Autonomous Underwater Vehicle (AUV) for wind farm inspection. This paper presents our design solutions for a jointed watertight AUV body made using current 3D printing techniques to achieves watertightness and resilient composite metal-polymer bonding. The design avoids dynamic interfaces and the need for rotary seals yet achieves robustness and strength. Test results prove a successful implementation of the magnetic connection between a freely rotating inner shaft and a driven outer shaft in a fish-like jointed AUV body.

Index Terms—AUV, Magnetic Joint, Robotic-Fish, 3D Printing

I. INTRODUCTION

Offshore wind generation, providing clean, reliable and commercially viable energy is projected to grow significantly in the coming years [1]. To ensure reliable production, regular Inspection Maintenance and Repair (IMR) tasks at high sea up to 100m depth need to be performed in a cost effective and safe manner. To extend Autonomous Underwater Vehicle (AUV) intervention time and perform IMR tasks the AUV needs to be efficient and flexible in operation. The vertebral column structure of a fish-like AUV is able to mimic propulsion techniques observed in nature and provides higher specific thrust efficiency at low swimming velocities during sensor data acquisition, higher physical mobility in limited spaces and low environmental footprint. The Authors' project "Autonomous
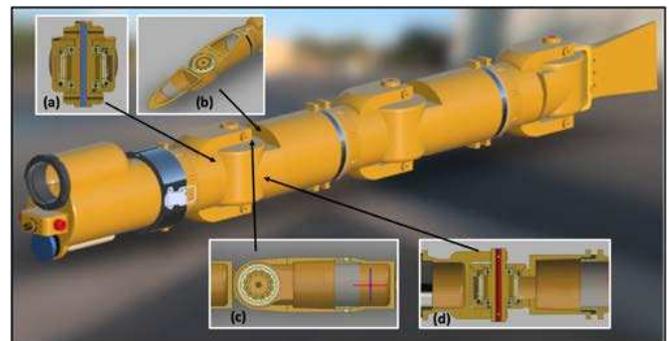
Fig. 1: The RoboFish under construction; (a) (b) (c) (d) perspectives of the magnetic joint cross sections

Biomimetic Robot-fish for Offshore Wind Farm Inspection", supported by the Supergen Renewable Energy Hub and the White Rose University Consortium, is specifically aimed at investigating and exploiting these advantages to facilitate autonomous inspection of offshore infrastructure.

However, splitting a protective, watertight enclosure into jointed segments, as shown in Fig. 1, brings many challenges to water tightness, particular in deep water under high pressure conditions. In the literature, smart materials [2] and structures [3] provide a potential solution to body flexibility, but often are still in the development stage and lack the required robustness. Many robotic projects [4] [5] rely on a watertight covers while others use a dynamic shaft seal [6].

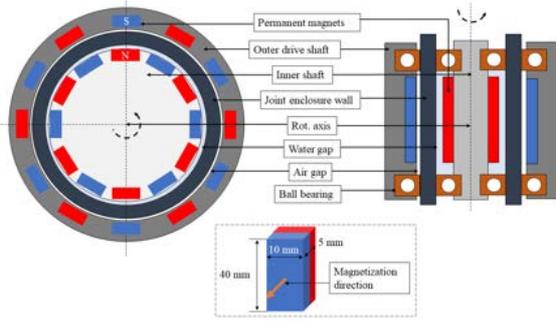To avoid weak points to water ingress such as dynamic

Fig. 2: Cross-section of magnetic joint and its components

Fig. 3: Magnet couple relative to the rotational axis

interfaces between moving elements of the watertight hull and watertight fastening of a cover, this work presents the design of an innovative, sealed joint via magnetic coupling, detailed in Fig. 1. A prototype was developed using inexpensive and accessible additive manufacturing techniques. This paper discusses the design, calculations and lessons learned while building a prototype using off the shelf parts together with a popular 3D printing processes. To the best knowledge of the authors, such a magnetic coupling has not been presented for a bio-inspired AUV in the literature, although similar magnetic clutches are widely proven in other industrial applications.

The paper is organised as following: section II introduces the magnetic joint design; section III discusses the RoboFish 3D printing process; section IV describes the assembly and finishing of one segment; section V presents test results of a segment; and finally, section VI concludes the paper.

The key contributions in the final paper will include:

- The detailed design for the innovative magnetic coupling
- Integration details for the use of this coupling in a bio-inspired AUV
- Shared lessons learned in the use of additive manufacturing of underwater parts

II. MAGNETIC JOINT DESIGN

A magnetic clutch provides a mechanical non-contact bond between two parts. The bond continues through fluids and solids that do not interrupt the magnetic field. The design processes focused on maximising the magnetic coupling force while remaining within the dimensions of the overall swimmer and keeping the weight as low as possible. To achieve this a design orientated model has been established to approximate the maximum transmittable torque of different number, type and arrangements of magnets. With the aim to reduce the cost of the prototype, only off the shelf block type magnets were considered. Figure 2 shows a schematic of the general arrangement of the designed clutch.

A. Magnet Calculation and Placement

A magnetic clutch makes use of the attracting forces of magnet couples of opposite polarity exerted in proximity. For the considered design all couples are positioned upright around a rotational axis with the polarisation vector intersecting the
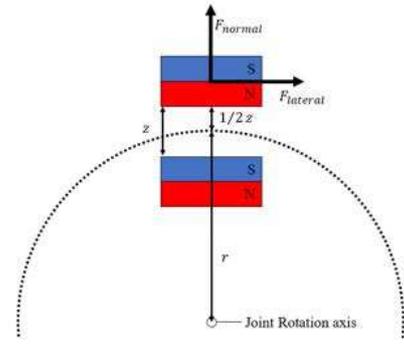
rotational axis. The magnet couples are fixed to a drive and driven shaft, respectively. The forces between the two magnets result in the transfer of torque between the shafts. The exerted normal and lateral forces depend on the dimensions, grade and the position of the magnet couples relative to each other. Figure 2 shows a schematic of such a magnet couple.

To approximate the normal force F_{normal} between two magnets for a specific gap size z and the maximum lateral force $F_{lateral,m}$ at the same distance, equations (1) and (2) published in [7]. Variable L_1 and L_2 is the length parallel to the lateral force vector, equal for both selected magnets. The coefficient F_0 and d_e are found using an online force calculator [8]. A comparison of the resulting force-distance curves has shown a good match with data of the reference publication. Equation (3) calculates the maximum transmittable torque τ_m before slip, where n is the number of magnet couples fixed to both shafts, and r the uniform radius equal to the middle distance between the magnet couple and the rotational axis.

$$F_{normal}(z) = \frac{d_e^2}{[z + d_e]} F_0 \qquad (1)$$

$$F_{lateral,m} = \frac{1}{1.11 - 0.244 \ exp\left(-2\left[\frac{L_1}{L_2} - 1\right]\right)} \frac{F_0}{L_2} \frac{d_e^2}{z + d_e} \qquad (2)$$

$$\tau_m = n \cdot F_{lateral,m} \cdot r \qquad (3)$$

The created joint design promises sufficient coupling force between a freely rotating inner shaft and servo driven outer shaft. Both components are physically separated by the water-tight enclosure, safely protecting the electronics components and leaving only the inner shaft exposed to water.

The joint provides 1 degree of freedom and can be installed for either yaw or pitch rotation by rotating it $90°$. The current version of the joint is connected to a digital servo. The torque between servo and outer shaft is transmitted via a HTD M5 profile timing belt using a gear ratio of pulley to shaft of ca. $\frac{1}{3}$ resulting in a maximum rotation of ca. $+-60°$ at increased torque and reduced velocity. Compared to rigid push pull rods or wires, a timing belt provides constant torque transmission.

TABLE I: RoboFish Joint design versions sorted from oldest to newest

Module	Material	Advantages	Disadvantages	Comments
	ASA	• Complexity: low - uses only 2 ball bearings; no magnets • Printability: high • Acetone: dissolves well • Accuracy: Very High • Strength: high • Stiffness: medium • Durability: medium	• Requiring rotary seals • Week rotary shaft • Unsuitable for high-torque servos • Tricky to print due to the high temperature resistance of ASA • Requires special model of printer to prevent internal stress during printing and layer separation	ASA has very high UV stability when exposed to sunlight. Parts can be easily sanded, painted, glued, drilled, and cut. Parts dissolve in acetone well, allowing layer lines easy to smooth
	ABS; PVC	• Complexity: Medium - requires 4 ball bearings and 24 magnets • Printability: medium • Acetone: dissolves well • Strength: medium • Stiffness: medium • Durability: High • Accuracy: Medium - also depends on printer calibration	• ABS to PVC interlocking parts require strong water-resistant adhesive • Joint housing printed in two parts due to the limited printer envelope size • O-rings unusable between ABS/PVC parts due to surface tolerances needed • Weak and breakable forks (orange) • 24 magnetic blocks of $40 \times 10 \times 5mm$	Tolerance of 0.5 mm, minimum wall thickness of 4 mm, and 100% infill recommended for underwater applications. Acetone used in post processing to smooth surfaces for glossy finish. Parts can be easily sanded and drilled
	PLA; 316 Stainless steel	• Complexity: medium • Printability: medium • Acetone: hardly dissolves • Strength: high • Stiffness: high • Durability: low • Accuracy: dependent upon printer calibration	• Harder to sand and soften surfaces • Stainless steel to PLA interlocking parts needs accurate interference fit • 4 corrosion-resistant ball bearings • 24 magnetic blocks of $40 \times 10 \times 5mm$	Tolerance of 0.5 mm, and a minimum wall thickness of 4 mm, and 100% infill recommended for underwater applications. Parts can be sanded and drilled, however greater care is needed.

III. 3D PRINTING PROCESSES

3D printing technologies such as Stereolithography (SLA) and Fused Deposition Modeling (FDM) are recognised for their ability to fast prototype. Popular in academia, industry and hobby applications. While the techniques are well understood and mechanical properties of the final part are rather predictable, achieving water tightness of a new design is a complex and multi-iteration process. Both techniques can generate complex physical models, yet FDM is usually less expensive. Additionally, the filaments used in FDM, compared to the liquid resins of an SLA printer, provide stronger mechanical properties and are less sensitive to environment media, for example sunlight. These conclude the main reasons for selecting FDM using Acrylonitrile Butadiene Styrene (ABS), Acrylonitrile styrene acrylate (ASA) and Polylactic acid (PLA) filament to print a RoboFish prototype. As shown in Fig. 1, the RoboFish follows a modular structure with each module being fully enclosed from the surrounding water. Fig. 5 shows the latest module, called segment, design, following the development of a number of experimental designs described in Table I. Printing watertight enclosures using FDM comes with several challenges, which will be discussed in the context of building a watertight prototype fitted with magnetic joints.

A. Printer Configuration

Printing outcomes depend on part geometry and print settings including nozzle size, infill and layer height. These parameters need to be found for a specific geometry and are often not transferable between printers. Additionally, high sensitivity to filament quality, room temperature amongst other difficult to control factors require detailed planning and care to achieve water tightness. The reason for water ingress can be structure imperfections, which can be caused by numerous factors. For the latest segment version, illustrated in Fig. 5, the print parameters are listed in Table II, which have given good results discussed in Section V.

B. Printer Tray Layout

This subsection discusses how component orientation on a printer tray affects accuracy, print time, strength and quality.

a) Component accuracy: When, for example, printing a hollow cylinder with FDM while positioning its centre axis vertical, the 3D printer will build it as a series of concentric circular layers on top of each another. This should result in a relatively smooth outer surface. If the same circular component is re-positioned with a horizontal centre axis, the built layers will take a rectangular shape with different widths to produce a cylinder. In this case, the resulted surface will be less smooth due to the change in layers width, plus the part of the surface that touches the printer tray will be flat. Therefore, orientation of the printed component plays a vital role in the print quality.

b) Printing time: Using the cylinder example again, the dimensions of the cylinder will determine which orientation would allow less manufacturing time. If the length of the cylinder is much greater than its diameter then printing in the horizontal orientation will take significantly less time than printing in the vertical. That is because of the total number of layers will be significantly smaller. For (100 mm outer diameter and 200 mm length) at a 100 μm layer height, the
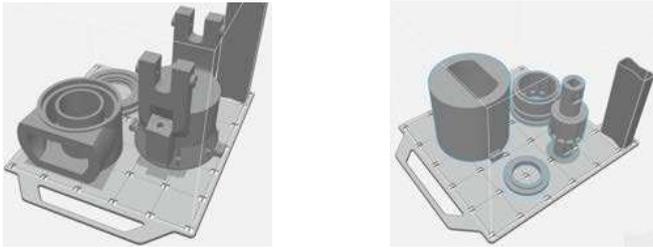
(a) 1st round components   (b) 2nd round components

Fig. 4: Printer tray layout and segment components orientation

(a) Joint Components   (b) Joint Assembled

Fig. 6: The latest 3D printed RoboFish segment after a number of redesign iterations following a series of laboratory tests

horizontal orientation will require 1000 total layers to print the cylinder, whereas the vertical will require 2000 layers. The time difference increases significantly with large components.

c) Part strength: Typically, the materials that are used in FDM have anisotropic properties. In other words, they are much stronger in the XY direction than the Z direction. For more durable parts, it is important to consider the application and torque. As a rule of thumb, components are more likely to withstand higher loads when the direction of the load is parallel to layers as opposed to normal to layers.

Planning the layout of the printer tray is an important factor. To print the RoboFish segment, illustrated in Fig. 5, the components are placed on the printer tray as shown in Fig. 4. The total print time per segment is 4.3 days, and the total print time for 5 segments is 21.5 days. The actual number of days will be longer than this, since when a print finishes, the next print cannot start before some cleaning and preparation work. The total manufacturing time can take up to 3-4 weeks.
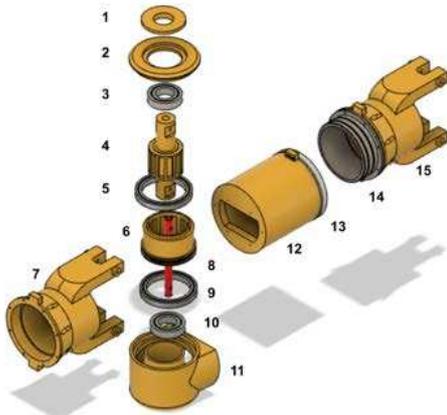

Fig. 5: All parts compromising one tested RoboFish segment: 1- Inner joint housing lid; 2- Outer joint housing lid; 3 & 10- Zirconia ceramic bearing; 4- Driven shaft; 5 & 9- Stainless bearing; 6- Driving shaft; 7 & 15- Electronic housing; 8- Reinforcement Aluminum bar; 11- Joint housing; 12- Servo housing; 13- Female Stainless ring; 14- Male Stainless ring

IV. ASSEMBLY AND FINISHING

All joint parts, shown in Fig. 5, are sized to fit. Post-print processing is an opportunity to fix shortcomings of the printing technique or the print itself. While the magnetic joint avoids dynamic interfaces, static part interfaces with non-permanent connections are needed for assembly and maintenance. The design geometry of modules is a cylinder for tolerance of high pressure in deep water, and uses two circular static interfaces, at the joint housing and halfway through the electronic housing in each module. O-rings at each provide a proven and inexpensive block to water ingress and work reliably under high pressure. To guarantee function, manufacturers have strict requirements on O-ring groove and bore dimensions and surface conditions (e.g. roughness and hardness). During printing, fused deposition of layers results in visible print seams that cannot satisfy surface condition requirements and result in uneven compression and leakage, even with small nozzles and after applying post processing techniques such as sanding or acetone treatment. To overcome this problem, 304 Stainless Steel rings machined to specification are glued to the printed parts at these interfaces with a two component epoxy. These are parts (13) and(14) in Fig. 5.

Components (11) and (12) in Fig. 5 are simply glued permanently using Solvent Cement adhesive providing strong bond to the model. All segment surfaces were sanded with 220 and 400 grain sandpaper for a smoother finish. Segments are designed for undersea use; therefore, exposed to water and subjected to hydrodynamic loads from swinging at speeds up to 0.17 sec/60° provided by a high torque servo (Hitec D-845WP). This necessitates the use of reinforced bonds between components (11) and (12). Six longitudinal stiffeners made of stainless-steel screws are used to strengthen the segment by fitting them inside the printed walls at the interface between the two components (11) and (12). Finally, applying epoxy after sanding the two lids (1) and (2) surface is an effective way to remove any irregularities before closing the joint housing (11) with the lids. The printed shafts (4) and (6) inside the joint housing are wet sanded with 220, 400 and 800 grain sandpaper to provide them with an interference fit to the bearing. Two corrosion-resistant bearings (3)(5)(9)(10) are installed on each shaft to allow smooth spinning. Magnetic blocks are glued using epoxy (Araldite Standard) to both
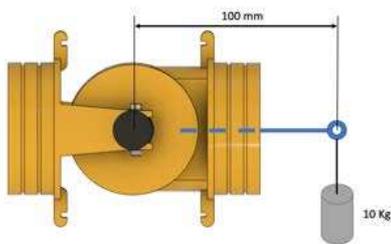
Fig. 7: With 9.96 Kg and 100mm lever the magnetic coupling between the 12 + 12 magnetic blocks breaks enabling emergency protection for the servo

shafts. This provides protection for the magnets exposed to water and bonds them well.

V. RESULTS OF A FULLY ASSEMBLED JOINT

This section provides some laboratory results of the latest 3D printed RoboFish segment, in terms of functionality and water-tightness. The latest segment, shown in Fig. 6, has been printed in APL, with print parameters listed in Table II.

A. Printing quality

Smooth rotation and use of off the shelf parts requires precise roundness and dimension tolerances, particularly to ensure correct position of the magnets with parallel placement between couples and minimizing the gap in between. It is known that ABS and PLA can produce accurate components, with printing details down to 0.8 mm and minimum features down to 1.2 mm. Despite this relatively wide tolerance allowance, the printed RoboFish components did not deviate more than ± 0.5 mm in the worst case. Some of the RoboFish printed components, the lids (1)(2) in Fig. 5, require an interference fit and adhesive after sanding. To this end, tolerance of 0.5 mm is recommended and using a minimum wall thickness of 1-2 mm ensures adequate strength in wall elements and bonds. Epoxy (Araldite Standard) has given excellent results with both ABS/APL materials.

It should be noted that the layer height could be made smaller, for a finer texture, although it is not clear whether or not that would improve water-tightness. It is possible that the layers might be better fused or the tiny gaps made smaller, but it might not make a difference to water ingress. However, this could produce a smoother surface finish to improve the effectiveness of a resin coating by creating smaller gaps to fill, but this is pure conjecture and may be tested in future prints.

TABLE II: List of the 3D printer parameters

Parameter	Value	Comment
Layer height	0.254 mm	Standard
extrusion width	0.5mm	Standard
Wall thickness	2.032 mm	To print more perimeters per layer
Solid infill	Enabled	To help preventing water ingress
Variable width fill	Enabled	To fill any small gaps
Room temperature	25°	Enclosure

(a) Ball Bearings

(b) Servo and Timing belt

Fig. 8: Tension is provided to timing belt using a 2-part sliding mounting comprising fixed and moving parts with two jack screws; two corrosion-resistant bearings are used on each shaft

B. Joint functionality

The magnetic attraction between the rotor and stater, components (4)(6) shown in Fig. 5, has been proven to be very powerful and confirms the function and strength of the magnetic joint design. With a 50 mm servo arm, the joint can rotate up to +/- 30 degrees which is sufficient for the design requirements of RoboFish. With a newer servo mounting, shown in Fig. 8, the tested segment can use a timing belt allowing larger joint rotation movement limited only by the servo range. The ball bearings were found in slightly loose-fitting in some pre-test prints. This is due to the relatively wide tolerance allowance and the high shrinkage of ABS, which can be compensated for in next prints. Alternatively, shimming material can be appended. In the latest print iteration, to overcome this tolerance issue, 0.25 was added or subtracted to the bearing mating surfaces and this proved sufficient for an interference fit.

Magnetic coupling breaking point: The servo torque is smoothly transferred to the outer shaft and further onto the inner shaft through the magnetic coupling. The joint's maximum transmittable torque before slip, or so called 'cogging', has been tested by fixing the inner shaft in place and attaching weights to a 100mm lever arm connected to the outer shaft. The result is shown in Fig. 7. This joint uses 12 magnetic blocks of $(40mm \times 10mm \times 5mm)$ on the rotor and an equal number on the stator. With a 100 mm lever, the magnetic coupling will break at approximately a 10 Kg load, as shown in Fig. 7. This is more than twice the satisfactory maximum torque for this application.

C. Water-tightness

FDM printed parts come with inevitable imperfections due to layer boundaries. Layer boundaries are mechanical weak points, and also have an impact on the fidelity of any geometry in the vertical plane. This is particularly visible with curves in the vertical plane, as it can be seen with some of the RoboFish curved structures. The layer boundaries lead to a "stepped" appearance in some corners, for example in Fig. 9, which is an early version of the RoboFish magnetic joint housing. Hence, for structurally important curves, the part orientation is set up in the printer so that the curved geometry is parallel to the print bed, because then the curves can be smooth and strong, as they are in the plane of the extruded filament and the fidelity

of the structure is limited only by the accuracy of the print head movement and the extrusion width, rather than by the layer boundaries. This was not possible with some versions of RoboFish parts, which is why some of the curves have a 'stepped' texture. The following solutions have been tried as practical solutions to this issue:

- Printing with 100% density infill, the part is nominally 'solid' and has no large hollow spaces inside. This has an impact on the weight and buoyancy of the RoboFish, which is important for other reasons that are out of the scope of this paper. By doing this, the interior of the parts should no longer be able to fill with water. However, due to the FDM process, tiny voids and gaps are still present in a 100% density print, and by itself this is not enough to solve the problem.
- Exposing the surfaces of the segment to acetone liquid or vapour inside a container, as shown in Fig. 10a. This caused the plastic at the surface to melt and fuse together, which helped to seal the layer boundaries and produce a much smoother finish.

Epoxy has also been applied in weak areas after sanding the component surfaces as it is an effective way to ensure 100% water-tightness. There is also a plan to apply bicomponent acrylic putty and sand it to repair printing imperfections.

The main body of the joint has a 120mm outer diameter with 4mm walls, allowing the use of 2 stainless steel rings to be used as a male-female connection and build a watertight interface with two O-rings. This provides a structural body reinforcement with water-tightness. The printed segments were submerged into a bathtub for more than 10 hours, see Fig. 10b, and no affect in material properties was observed. The segment is therefore assumed to be watertight at this low pressure.

VI. CONCLUSIONS

The presented work shows successful prototyping of a powerful and versatile magnetic joint coupling and provides discussion and identification of key factors for successful application of cost saving measures and easy accessible additive manufacturing methods for bio-inspired underwater robots. We have shared our experiences and lessons learned during the
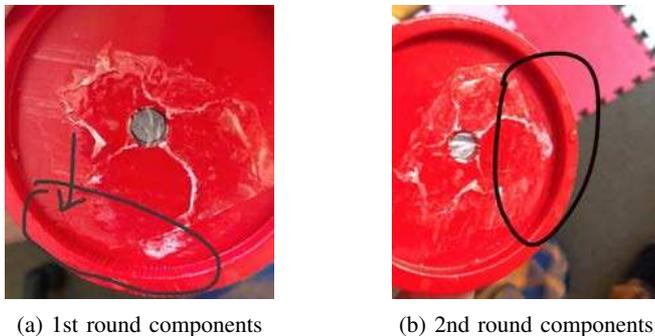

(a) 1st round components   (b) 2nd round components

Fig. 9: Early version of RoboFish magnetic joint showing imperfections due to layer boundaries

(a) Joint in Acetone 24 hrs   (b) Joint in Water 24 hrs
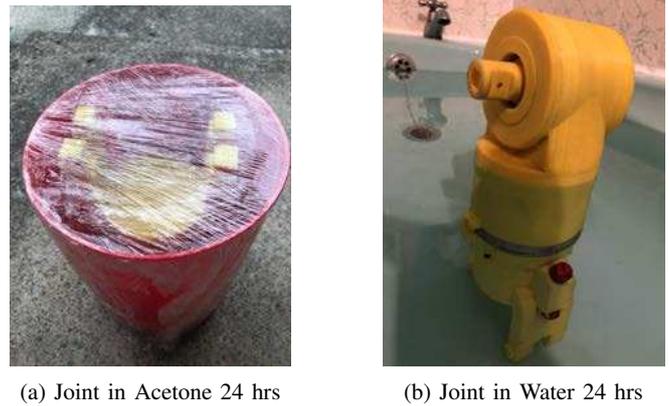
Fig. 10: Exposing the surfaces of a joint to acetone liquid or vapour. This causes the plastic at the surface to melt and fuse together. This helps to seal the layer boundaries and produce a much smoother finish and water-tightness

process of manufacturing a full RoboFish segment that uses this magnetic joint.

REFERENCES

[1] O. Catapult. (2020) Sme report: Offshore wind market. [Online]. Available: https://ore.catapult.org.uk/app/uploads/2018/10/OREC01_7468-SME-Report-2-Offshore-Wind-Market-SP.pdf

[2] N. Kamamichi, M. Yamakita, K. Asaka, and Z.-W. Luo, "A snake-like swimming robot using ipmc actuator/sensor," in *Proceedings 2006 IEEE International Conference on Robotics and Automation, 2006. ICRA 2006.* IEEE, 2006, pp. 1812–1817.

[3] K. W. Moored, F. E. Fish, T. H. Kemp, and H. Bart-Smith, "Batoid fishes: inspiration for the next generation of underwater robots," *Marine Technology Society Journal*, vol. 45, no. 4, pp. 99–109, 2011.

[4] F. Kirchner, S. Fechner, and D. Spenneberg, "Bio-inspired locomotion for underwater exploration and investigation," in *International Conference on Offshore Mechanics and Arctic Engineering*, vol. 47462, 2006, pp. 729–734.

[5] P. Liljebäck and R. Mills, "Eelume: A flexible and subsea resident imr vehicle," in *Oceans 2017-Aberdeen*. IEEE, 2017, pp. 1–4.

[6] B. Bayat, A. Crespi, and A. Ijspeert, "Envirobot: A bio-inspired environmental monitoring platform," in *2016 Ieee/Oes Autonomous Underwater Vehicles (Auv)*. Ieee, 2016, pp. 381–386.

[7] W. K. Schomburg, O. Reinertz, J. Sackmann, and K. Schmitz, "Equations for the approximate calculation of forces between cuboid magnets," *Journal of Magnetism and Magnetic Materials*, p. 166694, 2020.

[8] K. Magnetics. (2020) Magnetic force calculator. [Online]. Available: https://www.kjmagnetics.com/calculator.asp